Desalination and Water Treatment
www.deswater.com

doi:10.5004/dwt.2017.20394

72 (2017) 197–206
April

Properties of chemically prepared corncob-based activated carbons and their adsorption characteristics for aqueous lead and phenol

Qing-Song Liu

School of Water Resources and Environment, China University of Geosciences (Beijing), Beijing, 100083, China, Tel. +86-010-82322281, Fax +86-010-82321081, email: liukingsong@163.com

Received 12 April 2016; Accepted 9 September 2016

ABSTRACT

To study the effects of activator on the surface and adsorptive properties of activated carbons (ACs), corncob-based ACs were prepared using H_3PO_4, KOH and K_2CO_3 as activators. Their surface physic-chemical characteristics were analyzed using SEM, FTIR, XPS, XRD and BET methods. Compared to other ACs, H_3PO_4 activated AC (AC-PA) had more oxygen-related groups, more hydrophilic surface and larger surface area (680.7 m^2/g). Its pore size distribution was more heterogeneous. Resulted from the oxygen-containing and P-related groups, AC-PA gave favorable adsorption for Pb, with a maximum capacity of 298.5 mg/g. The adsorption of Pb onto other ACs was inferior and mainly through surface precipitation. Due to the combined effects of several interactions, the adsorption performance of ACs for phenol related to the concentration range. Surface properties including surface area, oxygen-containing groups and pore size distribution affected the interactions. AC-PA gave poor adsorption at low concentration but reached higher maximum uptake. Post-heat treatment of AC-PA strongly improved phenol adsorption especially at low concentration range. Accordingly, H_3PO_4 is more suitable to prepare ACs aiming at heavy metal removal. Other activators might be applicable when phenolic compounds are targeted. In addition, H_3PO_4 activation enjoyed the advantage of higher carbon yield.

Keywords: Activated carbon; Corncob; Surface characteristics; Lead; Phenol

1. Introduction

Activated carbons (ACs) are widely used for the removal of organic chemicals and heavy metals from drinking water and wastewater. Conventional raw materials for ACs preparation include wood, coal and coconut shell. Recently, the use of agricultural byproducts as raw materials for ACs has attracted an increasing attention, due to their renewability, abundance and low economic value. Corncob is a cheap and abundant agricultural waste. In China, its annual yield is estimated to be 20 million tons [1]. Corncob-based ACs have exhibited good adsorption performance for aqueous pollutants such as dyes, heavy metals, and organics [2–4].

There are two basic strategies for AC preparation: physical and chemical activation. Chemical activation involves impregnation of raw materials with activators followed by heat-treatment at moderate temperature (400~600°C) [5]. Various activators have been employed in the chemical activation of corncob-based ACs, including H_3PO_4 [6–8], KOH [2,9] and K_2CO_3 [10]. The activation mechanisms vary largely among these activators, resulting in ACs with different surface properties. Surface properties including surface area, pore size distribution, oxygen functionalities, hydrophilicity etc, are crucial in determining the performance of AC in aqueous adsorption [11]. Thus, the choice of activator is essential for the preparation of ACs with desired surface and adsorption characteristics. However, the effects of activator on the surface properties and water purification performance of corncob-based ACs have not been systematically studied before. Moreover, some important aspects such as carbon yield, which is closely related with the economics of AC preparation, have not been given attention.

In this study, three types of corncob-based ACs were prepared under identical conditions using H_3PO_4, KOH

*Corresponding author.

and K_2CO_3 as activators. Their surface physic-chemical properties were determined by various methods. Their adsorption characteristics towards aqueous pollutants were evaluated and correlated with the surface properties. Lead and phenol were chosen as the model pollutants. Lead belongs to a group of heavy metals which are highly toxic and commonly found in wastewater. Phenol is a typical of organic contaminant which is harmful and widely present in wastewater. The two pollutants are frequently employed to test the adsorption characteristics of ACs [12,13]. The results will help us to choose suitable activators in the preparation of ACs aimed at removing certain pollutants from water.

2. Materials and methods

2.1. Preparation of corncob-based ACs

Corncob was collected from Wuqiao county, Hebei province, China. It was firstly washed several times with distilled water and crushed into granules with a size of 12~40 mesh. Then, 10.0 g corncob was soaked in 100 mL solution containing activator for 72 h at room temperature. The weight ratio of activator to corncob was set as 1:2.5 for each activator. After soakage, the residual liquid was removed and the impregnated corncob was dried at 80°C overnight. Subsequently, the impregnated corncob was carbonized in a muffle furnace (Luoyang, China) at 500°C for 2 h, with a heating rate of 4°C/min. After cooling to room temperature, the products were washed repeatedly with distilled water to a constant conductance, grounded into powder and sieved to particle size below 80 mesh. The resulted ACs, denoted as AC-PA (H_3PO_4 activated), AC-PH (KOH activated) and AC-PC (K_2CO_3 activated), were stored in a desiccator for further use.

The carbon yield, i.e., weight ratio of the resulted AC to corncob on dry basis, was measured and recorded.

2.2. Characterization methods

Thermogravimetric analysis of the impregnated corncobs was performed on a ZRY-2P Thermal Analyzer (Shanghai, China) to understand their pyrolytic behaviors. The samples were heated from room temperature at a rate of 10°C/min in flowing N_2.

Surface morphology of ACs was analyzed by a scanning electron microscope (SEM, Zeiss Auriga FIB-SEM, Oberkochen, Germany).

The elemental analysis of C, H, O, N and S was carried out using an elemental analyzer (EA 3000, Eurovector, Milan, Italy). The analysis of surface functional groups was based on the Boehm titration method [14]. The pH_{PZC} values were determined according to a mass titration method [15]. These analysis were all performed in triplicate.

The FTIR analysis was conducted with a Nicolet Nexus 670 (Thermo Nicolet, Madison, Wis., USA). AC sample was mixed with KBr powder and pressed into pellets. The spectra were recorded from 4000 to 400 cm^{-1}, scans were taken at a resolution of 2 cm^{-1}.

The XPS analysis was conducted using a PHI5700 ESCA system (Physical Electronics, Chanhassen, Minn., USA) equipped with an Al Kα X-ray source (1486.6 eV). Pass energy was set as 178.95 and 22.35 eV for survey and high-resolution spectra, respectively. The spectra were calibrated by taking the graphitic peak as 284.6 eV. Atomic ratios were calculated from survey spectra by correcting the peak areas based on sensitivity factors. The high-resolution C1s spectra were analyzed using the XPSPEAK software, based on the Gaussian-Lorentzian (80%:20%) function after baseline subtraction with Shirley method.

X-ray diffraction (XRD) analysis was carried out using a Philips X'pert MPD powder diffractometer equipment (Philips, Eindhoven, Netherlands) with Cu Kα radiation (λ = 0.15406 nm).

The textural characteristics were analyzed with a Micromeritics ASAP 2020 (Micromeritics, Norcross, USA), using N_2 as the adsorbate at 77 K. The surface area (S_{BET}) was obtained using the BET equation, the total pore volume (V_T) was estimated at a relative pressure of 0.99. The pore size distribution was obtained based on the non-local density functional theory (NLDFT).

2.3. Adsorption procedure

The adsorption of lead and phenol from aqueous solutions by ACs was conducted by batch mode in stoppered flasks. Analytical grade phenol and $Pb(NO_3)_2$ were used as the adsorbate. The concentration of phenol and Pb^{2+} stock solution was 1000 mg/L. The pH of Pb^{2+} stock solution was adjusted to 3.0 via addition of HNO_3. For each test, 0.100 g AC was mixed with 100 mL solution and then shaken in a thermostatic shaker at 25 °C for 24 h, with a shaking rate of 120 rpm. The initial concentration range was 20~200 mg/L for phenol and 25~400 mg/L for Pb^{2+}. For phenol adsorption, the final pH was controlled at 6.0 ± 0.2 via addition of NaOH (0.1 mol/L). For lead adsorption, KOH or HNO_3 solution (0.1 mol/L) was added to adjust the final pH in the range of 4.0 ± 0.2. This range was chosen to prevent the formation of Pb^{2+} hydroxides at increased pHs, which might result in additional removal. All tests were repeated three times.

After contact, the supernatant was filtrated with 0.45 μm membrane filters, followed by the analysis of adsorbate. The uptake of adsorbate by per unit mass of AC at equilibrium, q_e (mg/g), was calculated by the following equation:

$$q_e = V \cdot \frac{(q_0 - q_e)}{m} \quad (1)$$

where q_0 is the initial concentration of adsorbate (mg/L), q_e is the equilibrium concentration of adsorbate (mg/L), V is the volume of solution (L), and m is the weight of AC (g).

2.4. Analysis of adsorbate

The concentration of phenol was determined colorimetrically at 510 nm using the 4-aminoantipyrine method. The concentration of lead was analyzed with inductively coupled plasma atomic emission spectrometry (ICP-AES).

3. Results and discussion

3.1. Thermal analysis and surface morphology

The carbon yields were measured as 45.1 ± 3.4%, 14.7 ± 1.9% and 19.7 ± 3.1% for AC-PA, AC-PH and AC-PC,

respectively. High carbon yields for H_3PO_4 activated ACs have been observed in previous studies [16,17].

Fig. 1 shows the DTG curves of pristine and impregnated corncobs. The weight loss of pristine corncob could be divided into two stages: 200~340°C and 340~430°C, which correspond successively to the decomposition of hemicellulose and cellulose [18]. The decomposition of lignin occurs in a wide temperature range up to around 500°C. For H_3PO_4 impregnated corncob (CPA), the decomposition starts at a notably lower temperature (around 130°C). On its DTG curve, except the peaks relating to hemicellulose and cellulose decomposition, a broad peak is observed in the range of 400~700°C. For KOH impregnated corncob (CPH), the onset temperature of decomposition is also lowered. A sharp peak centered at around 250°C is coupled with a shoulder from 275°C to 375°C. The decomposition is so intense that the weight loss peaks of various components could hardly be distinguished. However, the weight loss rate is minimal above 400°C. For K_2CO_3 impregnated corncob (CPC), two strong neighboring peaks centered at around 250°C and 280°C are observed. Due to the decomposition of carbonate [19], appreciable weight loss occurs for CPH and CPC above 600°C with similar magnitude.

The chemical activation mechanisms of carbonaceous materials have been studied already. Phosphoric acid acts as an acidic catalyst to promote bond cleavage and crosslink formation, through reactions such as cyclization and condensation. Reacting with organic species, H_3PO_4 forms phosphate and polyphosphate bridges that connect and crosslink biopolymer fragments [20]. The catalysis effects result in lowered decomposition temperature. The formation of phosphate linkages prevents over decomposition, which is the intrinsic reason for a higher carbon yield of AC-PA. As suggested by DTG curve, the decomposition rate of CPA below 400°C is much lower compared to other samples. However, the polyphosphate linkages start to decompose at elevated temperature, leading to a continuous weight loss in the temperature range of 400~700°C.

A series of complex chemical reactions occur in KOH activation. Generally, the primary reactions could be expressed as follows [19,21]:

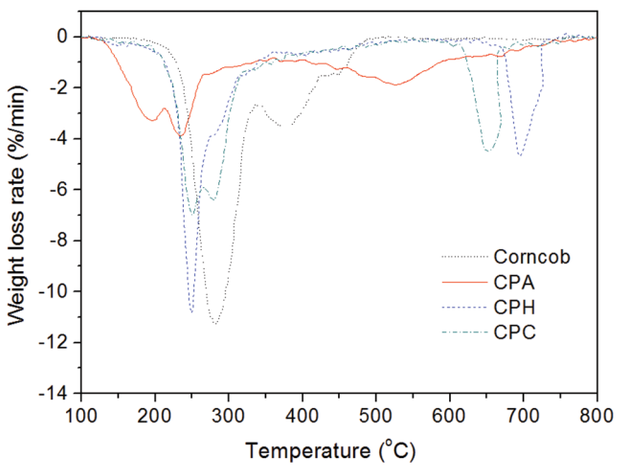

Fig. 1. DTG curves of pristine and impregnated corncobs.

$$4KOH + -CH_2 \rightarrow K_2CO_3 + K_2O + 3H_2 \quad (2)$$

$$K_2CO_3 + 2C \rightarrow 2K + 3CO \quad (3)$$

$$K_2O + C \rightarrow 2K + CO \quad (4)$$

$$K_2O + CO_2 \rightarrow K_2CO_3 \quad (5)$$

$$2K + CO_2 \rightarrow K_2O + CO \quad (6)$$

$$CO_2 + C \rightarrow 2CO \quad (7)$$

The complex reactions between hydroxyl ions, K-containing species and the lignocellulosic material lead to the decomposition of precursor and the development of porosity. The fierce reactions undergo almost indiscriminately for various components in corncob matrix. The intense weight loss is associated with OH^- and CO_3^{2-} anions through reactions (2) and (3). It was reported that K_2CO_3 was formed at around 400°C [19]. According to reactions (4) to (6), K-containing species and K metal participate in cyclic redox reactions, resulting in the consumption of precursor. The generated potassium metal may intercalate into the carbon matrix, resulting in the widening of spaces between carbon layers [22]. According to reaction (7), the released CO_2 in the system also makes contribution to porosity development. However, KOH does not act to crosslink various fragments and to prevent over decomposition, leading to a lower carbon yield of AC-PH.

The impregnation of K_2CO_3 also modifies the carbonization behavior. Reaction (3) is the primary reaction initializing the activation process. Obviously, some reactions are similar between K_2CO_3 and KOH activation. However, as OH^- is substituted by CO_3^{2-}, their activation mechanisms differ in some respects. The weight loss of CPC is not as fierce as CPH at temperature range 200~300°C, implying the importance of reaction (2) in the decomposition of CPH. Furthermore, the decomposition temperature of carbonate for CPC is lower than that for CPH, since K_2CO_3 is readily available on CPC surface.

The SEM images of three ACs with different magnifications are shown in Fig. 2. These images reveal notable differences among them. In general, honeycomb shaped holes inherited from the precursor are observed on each AC. The holes on AC-PA, with diameters of 20~50 μm, are more regular and well arranged. Secondary holes with diameters on the order of 1 μm are evident. On the contrary, the holes on AC-PH and AC-PC are discrepant in size and surrounded by deformed and twisted walls. This observation confirms that the structure of corncob is damaged more severely when KOH and K_2CO_3 are employed. Moreover, a large amount of defects with diameters of 1~3 μm are obvious on AC-PH, most of them form clusters. These defects are derived from the strong etching of KOH. In fact, the surface morphology also implies serious burn-off of CPH and CPC during activation.

3.2. Surface chemical properties of ACs

Table 1 presents the elemental analysis of C, O, H, N and S in corncob and AC bulk. C, O and H are the major

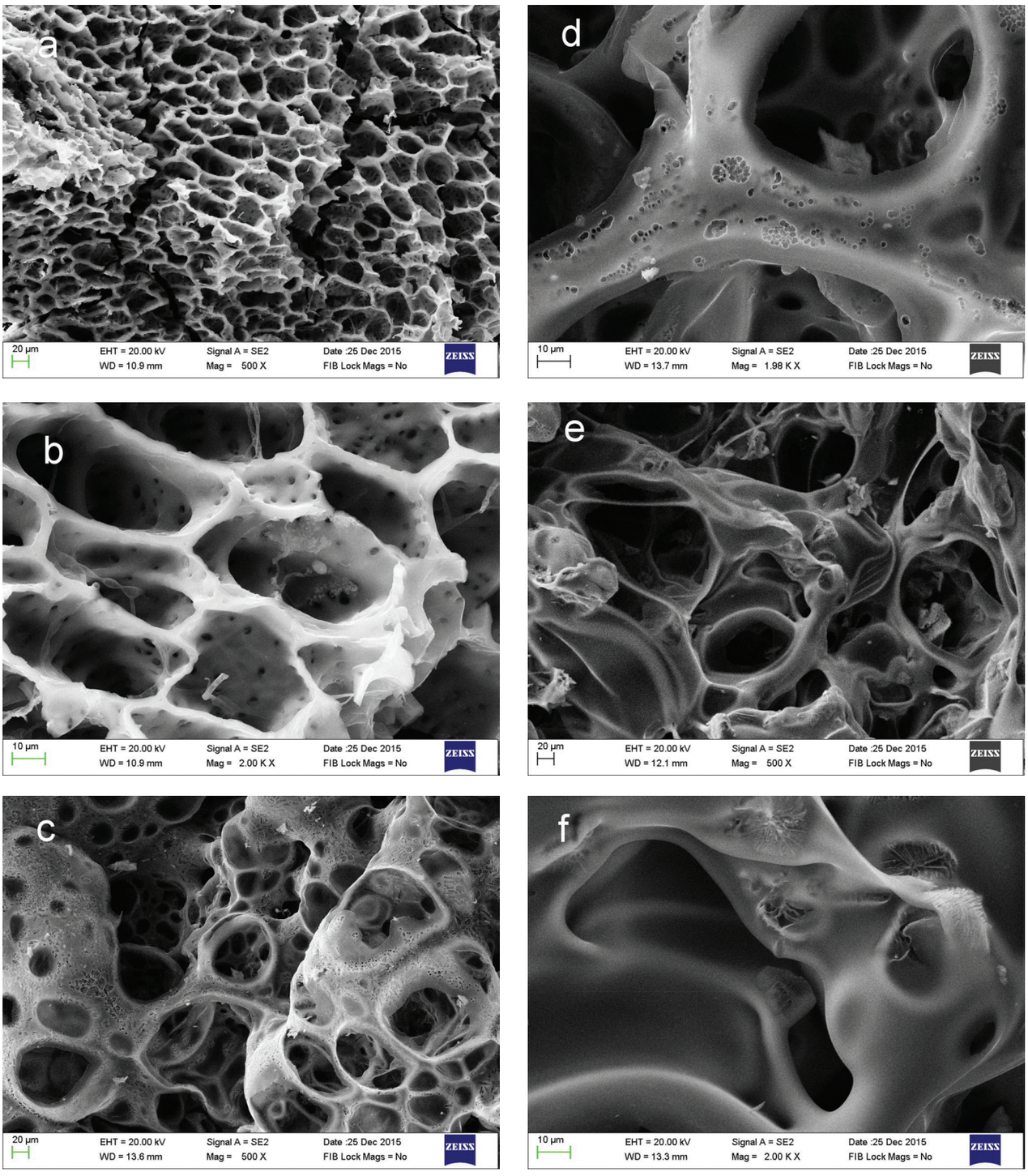

Fig. 2. SEM images of ACs: (a,b) AC-PA, (c,d) AC-PH, (e,f) AC-PC.

elements for these samples. Compared to the precursor, the C contents of ACs show a notable increase, while the heteroatoms exhibit a substantial decrease. Atomic ratios of elements are calculated to estimate the characteristics of ACs. Decreased H/C atomic ratios are observed for ACs, suggesting that the precursor lose aliphatic and forms aromatic structure during activation [23]. With much lower H/C ratios, AC-PH and AC-PC are more aromatic than AC-PA. The O/C atomic ratios decrease for ACs, indicating the removal of oxygen-related groups. A decrease in this ratio reflects an increase in hydrophobicity [24]. Also, the O/C ratio of AC-PA is much higher than those of other ACs.

Table 1
Elemental analysis of ACs and corncob

Samples	C	O	H	N	S	H/C	O/C
Corncob	44.60	44.94	3.37	0.51	0.77	0.076	1.01
AC-PA	61.59	23.32	2.59	0.39	0.33	0.042	0.38
AC-PH	85.58	6.49	2.32	0.22	0.27	0.027	0.076
AC-PC	85.72	6.70	2.23	0.21	0.28	0.026	0.078

Due to the crosslink of phosphate and polyphosphate, more heteroatoms especially oxygen are retained after activation.

Table 2 lists the quantitative analysis of surface functional groups based on Boehm titration. Accordingly, there are abundant acidic groups on AC-PA (4.4 meq/g), most of which are carboxylic groups. The total amounts of acidic groups on other ACs are less, but the strong acidic groups always comprise the major portion. AC-PC has more carboxylic groups than AC-PH, although their total acidic groups are similar. The amounts of basic groups for AC-PH and AC-PC are close, i.e., 0.7 meq/g.

Table 2
Surface functional groups on ACs based on Boehm titration

Samples	Carboxylic (meq/g)	Lactonic (meq/g)	Phenolic (meq/g)	Basic (meq/g)
AC-PA	3.7	0.3	0.4	0.1
AC-PH	1.2	0.2	0.4	0.7
AC-PC	1.7	0.1	0.1	0.7

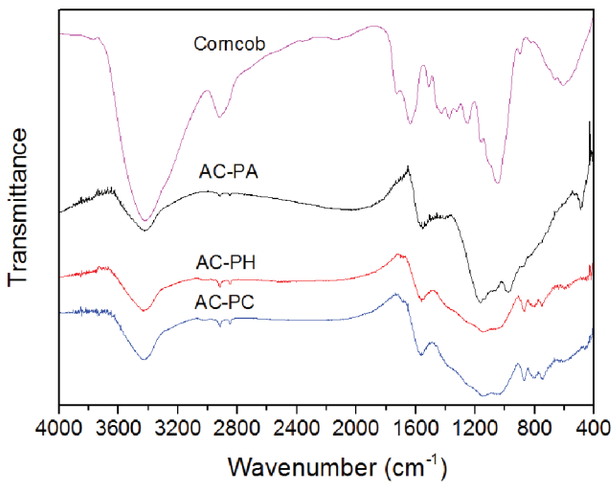

Fig. 3. FTIR spectra of corncob and ACs.

The pH_{PZC} values are 1.95, 9.15 and 9.20 for AC-PA, AC-PH and AC-PC, respectively. The low pH_{PZC} of AC-PA is resulted from the dominance of acidic groups, while the opposite is true for other ACs.

The FTIR spectra of corncob and various ACs are presented in Fig. 3. The strong bands at 3420~3430 cm^{-1} are assigned to O–H stretching of hydroxyl groups. The bands at around 2920 and 2850 cm^{-1} are attributed to aliphatic C–H stretching. A band at around 3020 cm^{-1} corresponding to aromatic C–H stretching is discernible for AC-PH and AC-PC. The strong bands at around 1560 cm^{-1} for ACs correspond to aromatic C=C skeletal stretching [25]. For AC-PA, the bands at 1163 and 974 cm^{-1} are characteristic of P-containing groups, including phosphate and P–OR esters. Puziy et al. [26] proposed that P was present in the forms of C–O–P and C–P–O. For AC-PH and AC-PC, bands at around 1150 cm^{-1} and 740~870 cm^{-1} are associated with the deformation vibration and out-of-plane bending of aromatic C–H. Accordingly, AC-PH and AC-PC show a higher aromaticity compared to AC-PA. For the precursor, a series bands in the range of 1050~1730 cm^{-1} are associated with C–H, C–O and O–H bonds. Their disappearance in ACs indicates the cleavage of these bonds during activation. Probably derived from its low content, the peak corresponding to carboxylic groups at around 1720 cm^{-1} could not be discerned.

XPS is useful for analyzing the surface chemistry of carbon materials. The relative contents of various elements on carbon surface, obtained from the survey scan, are tabulated in Table 3. Compared with elemental analysis (Table 1), the contents of C and O show the same trend after activation and among the ACs. Moreover, a fraction of residual P is observed on AC-PA; K is detected on other ACs, resulted from the impregnation of KOH or K_2CO_3. Some deviations

Table 3
Relative contents of elements on ACs surface based on XPS

Samples	C	O	P	K	Si	S	N
Corncob	76.77	21.33	ND[a]	ND	0.41	ND	1.49
AC-PA	80.45	16.31	2.52	ND	0.73	ND	ND
AC-PH	88.93	9.26	ND	0.72	0.73	0.31	ND
AC-PC	88.84	9.89	ND	0.73	0.40	0.15	ND

[a]ND means not detected.

are noticed between Tables 1 and 3, especially for corncob and AC-PA. Similar phenomenon were observed in other studies [27], indicating that the elemental compositions are not identical on the surface and in the bulk, as XPS method probes only several nanometers in depth [28].

The high-resolution spectra of C1s and O1s are given further analysis. Three components are considered for C1s with chemical shifts as: graphite (284.6 eV), C–OH (286.1 ± 0.1 eV), C=O (288.2 ± 0.1 eV) [29]. The following chemical shifts are considered for O1s: C=O (531.1 ± 0.1 eV), C–O (532.7 ± 0.1 eV), chemisorbed oxygen (534.1 ± 0.2 eV) [30]. The fitting curves are illustrated in Fig. 4, and the relative contents of various groups are tabulated in Table 4. Based on C1s analysis, the C–C contents of ACs are remarkably increased compared to corncob, indicating the formation of graphite after activation. Compared to other ACs, AC-PA shows higher contents of oxygen-related groups, which influence its surface hydrophilicity, ion exchange and other characteristics. According to O1s analysis, the relative C=O contents of AC-PH and AC-PC are higher than that of AC-PA. The C=O bond is associated with carboxyl and carbonyl groups, which probably account for the strong acidic groups measured in Boehm titration.

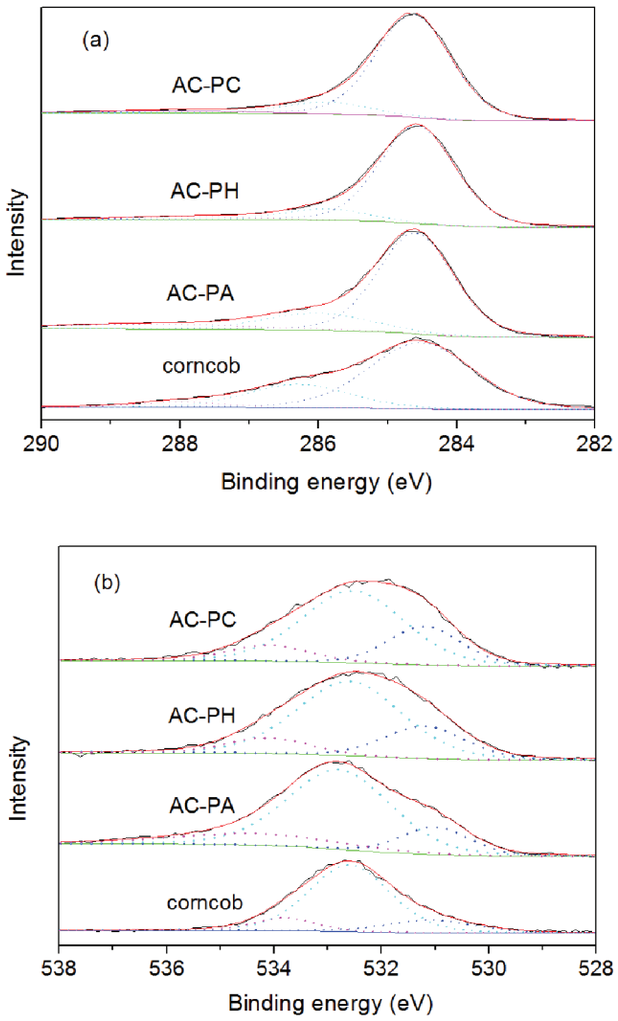

Fig. 4. High-resolution spectra curve-fittings: (a) C1s and (b) O1s.

Fig. 5 shows the XRD patterns of various samples. A peak at $2\theta \approx 22^{o}$ corresponding to the crystalline region of cellulose [31] is prominent for the precursor. For ACs, two broad diffraction peaks at $2\theta \approx 24^{o}$ and $\approx 44^{o}$ are attributed to the (002) and (10) diffraction of disordered micrographite stacking. The interlayer spacings of various ACs (d_{002}) are quite close (around 0.37 nm). The results prove a partial graphitization of ACs.

3.3. Textural properties of ACs

The textural parameters of various ACs are summarized in Table 5. The surface areas are 680.7, 385.6 and 332.3 m^2/g for AC-PA, AC-PH and AC-PC, respectively. The pore volumes are 0.297, 0.176 and 0.151 cm^3/g, respectively. The obtained surface areas for AC-PH and AC-PC are relatively low. Accordingly, their porous structure is not fully developed. The main reason should be attributed to the lower activation temperature employed in this study (500°C). Hayashi et al. [32] found that the activation of AC using KOH or K_2CO_3 obtained low surface area at 500°C.

The pore size distributions of various ACs are given in Fig. 6. The values of incremental pore volume prove a more developed porosity of AC-PA. As can be seen, four peaks are discernible for each AC: ultra-micropores centered at 0.5~0.6 nm, fine-micropores centered at 0.7~0.8 nm, super-micropores centered at 1.1~1.2 nm and 1.6~1.8 nm. For AC-PA, the super-micropores represent a high ratio, with substantial ultra- and fine-micropores. The narrow micropores are presumed to be resulted from the space occupied by P-containing groups after their removal through washing, while the wide micropores and mesopores are related to the decomposition of lignocellulosic materials catalyzed by phosphoric acid [33]. For AC-PH, the primary portion centers at 1.1 nm, with considerable ultra- and fine-microp-

Table 4
Relative contents of various groups based on C1s and O1s analysis

Samples	C1s			O1s		
	C–C	C–O–R	C=O	C=O	C–O	Chemisorbed
Corncob	66.66	28.47	4.87	15.87	73.08	11.05
AC-PA	78.02	16.96	5.03	15.89	68.49	15.62
AC-PH	85.73	10.68	3.58	22.48	66.38	11.13
AC-PC	85.37	11.47	3.16	23.29	66.43	10.28

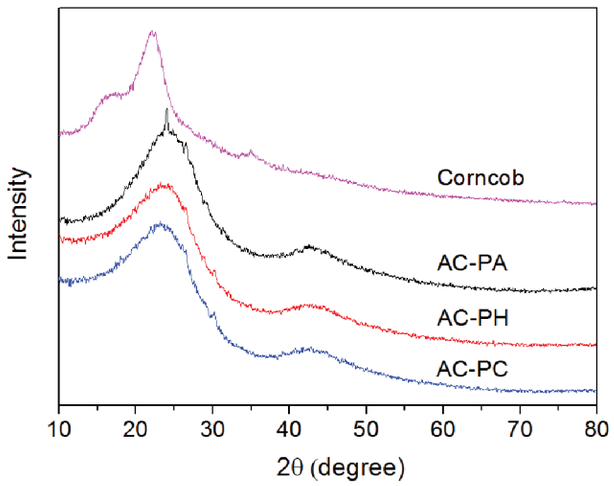

Fig. 5. XRD patterns of corncob and ACs.

Table 5
Textural parameters of ACs

Samples	S_{BET} (m^2/g)	S_{mic} (m^2/g)	V_T (cm^3/g)	V_{mic} (cm^3/g)
AC-PA	680.7	581.2	0.297	0.256
AC-PH	385.6	351.4	0.176	0.142
AC-PC	332.3	223.6	0.151	0.123

ores. AC-PC shows a distinct porosity strongly centered at super-micropores in the range of 1.0~1.3 nm. It is possible that CO_3^{2-}, which has larger dimension than OH^-, enlarges the narrow pores into wider ones, and/or the converted CO_2 exerts the same function.

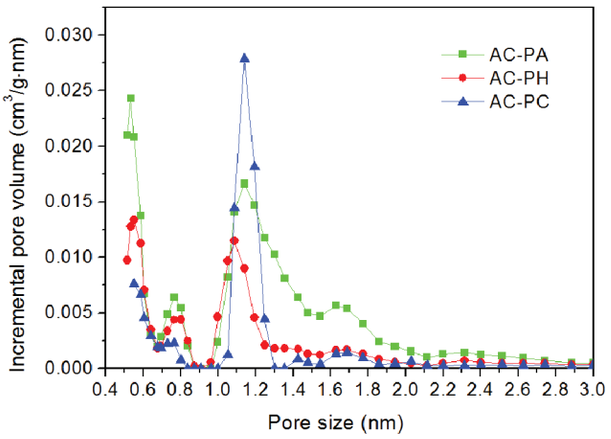

Fig. 6. Pore size distributions of ACs.

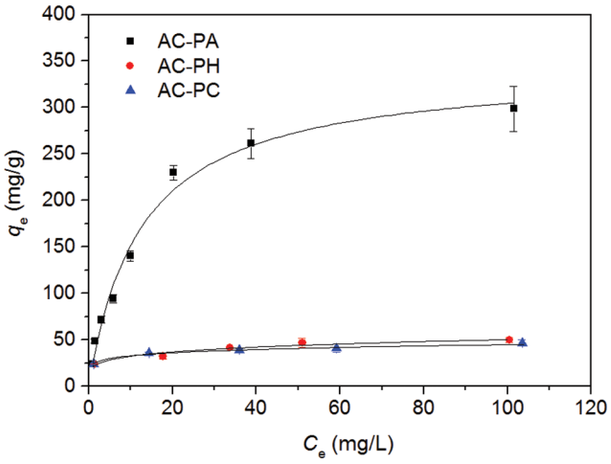

Fig. 7. Adsorption isotherms of lead on ACs at 25°C.

4. Adsorption characteristics of ACs for aqueous pollutants

4.1. Adsorption of lead

The adsorption isotherms of lead on various ACs are illustrated in Fig. 7. Obviously, lead adsorption on AC-PA is much stronger than on other ACs. A remarkable experimental uptake of 298.5 mg/g is achieved by AC-PA. Lead adsorption on AC-PH and AC-PC is favorable at low concentration range, but the isotherms rapidly reach a plateau. To explore the effects of porosity, the maximum uptake is divided by surface area. The values are calculated as 438.5, 128.4 and 135.4 μg/m^2 for AC-PA, AC-PH and AC-PC, respectively. Obviously, lead adsorption is related not only to the porosity, but also to the surface chemistry. The presence of abundant acidic surface groups on AC-PA endows it with greater ability for lead adsorption. Cation exchange, electrostatic force and surface complexation are generally accepted as the main mechanisms for lead adsorption [4,34,35]. With more acidic surface groups, AC-PA has a larger cation-exchange capacity. Lead is readily exchanged with some cations formerly present on its surface. At the experimental pH, AC-PA is negatively charged (pH > pH_{PZC}), resulting in electrostatic attraction towards Pb^{2+}. Surface complexation between Pb^{2+} and oxygen-containing groups, including carboxylic, carbonyl and phenolic groups, is also possible.

The discrepancies in the maximum uptake, as well as isotherm shape, indicate that the adsorption mechanisms vary largely between AC-PH, AC-PC and AC-PA. In fact, surface precipitation is probably the main mechanism for AC-PH and AC-PC, which explains for the favorable adsorption in low concentration range. Some anions on AC surface, such as OH^- and CO_3^{2-}, participate in these reactions. A plateau is reached after their consumption. Although the total acidic surface groups on AC-PH and AC-PC are around 40% of that on AC-PA (Table 2), their contribution in lead adsorption is minor, as suggested by the low maximum uptakes (49.5 and 45.0 mg/g for AC-PH and AC-PC, respectively). The electrostatic force is actually repulsive in nature between Pb^{2+} and AC-PH or AC-PC, since their pH_{PZC} values are above the experimental pH. Consequently, cation exchange and possible surface complexation are diminished. However, these factors could not explain the notable discrepancies in the maximum uptakes. As a matter of fact, the P-related groups are probably involved in lead adsorption on AC-PA,

through surface precipitation and electrostatic force. The presence of substantial P-related groups on AC-PA has been confirmed by the XPS and FTIR studies.

4.2. Adsorption of phenol

The adsorption isotherms of phenol on various ACs are presented in Fig. 8. As can be seen, the adsorption performance of ACs vary with equilibrium concentration. At low concentration range, the affinities of ACs towards phenol follow the order of AC-PH > AC-PA > AC-PC; at high concentration range, AC-PA is superior to other ACs, which give similar performance. The results imply that phenol adsorption involves different interactions. The π-π interactions between the aromatic ring of phenol and the graphene layer have been widely accepted as an important mechanism [36]. Other factors including surface functional groups, surface area and pore size distribution affect phenol adsorption to some extent. The prevalence of oxygen-containing groups on AC-PA surface lowers the density of π electrons, thus reduces the π–π interactions. Furthermore, they form water clusters at the entrance of pores through hydrogen bonding, making them inaccessible for phenol molecules. The poor performance of AC-PC at low concentration range relates to its porosity characteristics. With a surface area similar to that of AC-PH, AC-PC has less ultra- and fine- micropores. These narrow micropores retain phenol through "micropore filling" mechanism, resulting in favorable adsorption at low concentration range. However, the importance of oxygen-containing groups and pore size distribution diminishes with the increase of concentration, while surface area exerts ever enhanced effects. Hence, AC-PA, with the highest surface area, exhibits higher uptakes at high concentration range. The maximum uptakes of phenol are also divided by surface area. The results are 151.5, 230.3 and 257.3 μg/m² for AC-PA, AC-PH and AC-PC, respectively. Accordingly, the surface density of phenol on AC-PA is remarkably lower than those of other ACs.

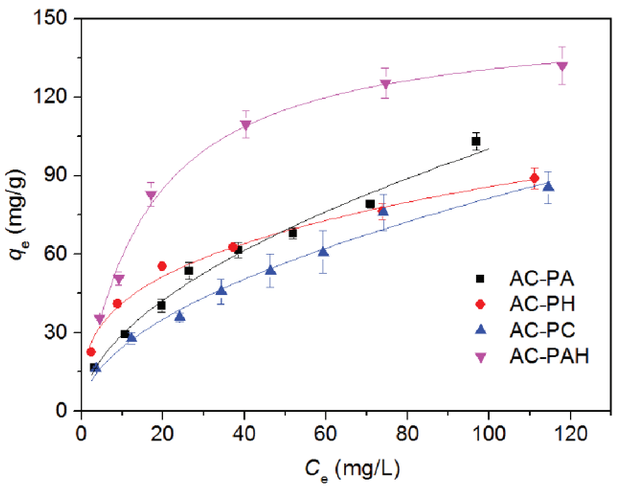

Fig. 8. Adsorption isotherms of phenol on ACs at 25°C.

Additional effort was made to improve the adsorption performance of AC-PA. After repeated washing and drying, AC-PA underwent post-heat treatment at 600°C for 2 h. The adsorption isotherm of phenol on the resulted AC, denoted as AC-PAH, is also shown in Fig. 8. The surface density of phenol on AC-PAH reaches 194.1 μg/m², notably higher than that on AC-PA but still lower than those on other ACs. The approximation of phenol density among various ACs suggests that surface area is more important in phenol adsorption than in lead adsorption. A more striking difference between AC-PAH and AC-PA lies in their performance at low concentration range. Phenol adsorption onto AC-PAH is strongly improved at this range, even much better than that of AC-PH. The amounts of carboxylic, lactonic and phenolic groups for AC-PAH, determined by Boehm titration, are 3.2, 0.2 and 0.3 meq/g, respectively. The decomposition of some acidic groups makes contribution to its improved performance. A comparison between AC-PA and AC-PAH supports the presumption that the adverse effects of oxygen-containing groups are more evident at low concentration range.

The widely used Langmuir and Freundlich models are applied to fit the isotherms. Langmuir model assumes a homogeneous adsorbent surface with identical adsorption sites, which can be written as:

$$q_e = q_m K_L C_e / (1 + K_L C_e) \quad (8)$$

where q_m is the maximal adsorption capacity, K_L is a constant related to the free energy of the adsorption.

Table 6
Model fitting parameters for the adsorption of lead and phenol onto ACs

Adsorbate	Adsorbent	Langmuir			Freundlich		
		q_m (mg/g)	K_L (L/mg)	R^2	K_F (mg/g)(L/mg)$^{1/n}$	n	R^2
Lead	AC-PA	342.8	0.0791	0.988	56.34	2.61	0.914
Lead	AC-PH	44.7	0.6360	0.725	20.68	5.21	0.950
Lead	AC-PC	41.4	1.0432	0.890	23.87	7.35	0.989
Phenol	AC-PA	143.6	0.0202	0.947	8.53	1.87	0.987
Phenol	AC-PH	100.0	0.0624	0.930	19.87	3.15	0.988
Phenol	AC-PC	126.2	0.0176	0.960	7.29	1.91	0.985
Phenol	AC-PAH	150.9	0.0645	0.994	27.49	2.91	0.935

Freundlich model is an empirical equation that can be written as:

$$q_e = \frac{q_m K_L C_e}{(1 + K_L C_e)} \quad (9)$$

where K_F and n are constants related to the adsorption capacity and adsorption intensity, respectively.

The model parameters are given in Table 6. The Freundlich model gives a better fitting for each case. The Freundlich model is considered to be applicable for highly heterogeneous surfaces, whereas the Langmuir is suitable for homogeneous surfaces [37]. Accordingly, the ACs used in this study have heterogeneous surface.

5. Conclusions

The different activation mechanisms of H_3PO_4, KOH and K_2CO_3 result in varied carbon yields and pyrolytic behaviors. Elemental analysis reveals the increase in C and the decrease in heteroatoms after activation, and remarkable variations between AC-PA and other ACs. AC-PA owns abundant acidic groups, while AC-PH and AC-PC have substantial basic groups. FTIR and XPS analysis demonstrate the presence of various groups. XRD studies prove a partial graphitization of ACs. Lead adsorption on AC-PA is much more favorable, due to its oxygen-containing and P-related groups. Phenol adsorption on ACs involves π–π interactions, physical force and surface functional groups. Consequently, the performance of AC depends on equilibrium concentration. A post-heat treatment of AC-PA improves its phenol adsorption at the whole concentration range.

Acknowledgements

The authors appreciate the financial support by the Fundamental Research Funds for the Central Universities (No. 2652015129).

References

[1] W. Li, Q. Li, L.Y. Zheng, Y.Y. Wang, J.B. Zhang, Z.N. Yu, Y.L. Zhang, Potential biodiesel and biogas production from corncob by anaerobic fermentation and black soldier fly, Biores. Technol., 194 (2015) 276–282.

[2] F.C. Wu, P.H. Wu, R.L. Tseng, R.S. Juang, Preparation of novel activated carbons from H_2SO_4-pretreated corncob hulls with KOH activation for quick adsorption of dye and 4-chlorophenol, J. Environ. Manage., 92 (2011) 708–713.

[3] R.L. Tseng, S.K. Tseng, Pore structure and adsorption performance of the KOH-activated carbons prepared from corncob, J. Colloid Interface Sci., 287 (2005) 428–437.

[4] A.N.A. El-Hendawy, Influence of HNO_3 oxidation on the structure and adsorptive properties of corncob-based activated carbon, Carbon, 41 (2003) 713–722.

[5] A.A. Ahmad, B.H. Hameed, Fixed-bed adsorption of reactive azo dye onto granular activated carbon prepared from waste, J. Hazard. Mater., 175 (2010) 298–303.

[6] N.V. Sych, S.I. Trofymenko, O.I. Poddubnaya, M.M. Tsyba, V.I. Sapsay, D.O. Klymchuk, A.M. Puziy, Porous structure and surface chemistry of phosphoric acid activated carbon from corncob, Appl. Surf. Sci., 261 (2012) 75–82.

[7] V.O. Njoku, B.H. Hameed, Preparation and characterization of activated carbon from corncob by chemical activation with H_3PO_4 for 2,4-dichlorophenoxyacetic acid adsorption, Chem. Eng. J., 173 (2011) 391–399.

[8] G.Z. Zhu, X.L. Deng, M. Hou, K. Sun, Y.P. Zhang, P. Li, F.M. Liang, Comparative study on characterization and adsorption properties of activated carbons by phosphoric acid activation from corncob and its acid and alkaline hydrolysis residues, Fuel Process. Technol., 144 (2013) 255–261.

[9] Y.X. Wang, B.S. Liu, C. Zheng, Preparation and adsorption properties of corncob-derived activated carbon with high surface area, J. Chem. Eng. Data, 55 (2010) 4669–4676.

[10] Y. Sun, P.A. Webley, Preparation of activated carbons with large specific surface areas from biomass corncob and their adsorption equilibrium for methane, carbon dioxide, nitrogen, and hydrogen, Ind. Eng. Chem. Res., 50 (2011) 9286–9294.

[11] C.O. Ania, B. Cabal, C. Pevida, A. Arenillas, J.B. Parra, F. Rubiera, J.J. Pis, Effects of activated carbon properties on the adsorption of naphthalene from aqueous solutions, Appl. Surf. Sci., 253 (2007) 5741–5746.

[12] A.H. Sulaymon, D.W. Abbood, A.H. Ali, A comparative adsorption/biosorption for the removal of phenol and lead onto granular activated carbon and dried anaerobic sludge, Desal. Water Treat., 51 (2013) 2055–2067.

[13] M. Caccin, M. Giorgi, F. Giacobbo, M. Da Ros, L. Besozzi, M. Mariani, Removal of lead (II) from aqueous solutions by adsorption onto activated carbons prepared from coconut shell, Desal. Water Treat., 57 (2016) 4557–4575.

[14] H. Boehm, Some aspects of the surface chemistry of carbon blacks and other carbons, Carbon, 32 (1994) 759–769.

[15] J.S. Noh, J.A. Schwarz, Estimation of the point of zero charge of simple oxides by mass titration, J. Colloid Interf. Sci., 130 (1989) 157–164.

[16] D. Prahas, Y. Kartika, N. Indraswati, S. Ismadji, Activated carbon from jackfruit peel waste by H_3PO_4 chemical activation: Pore structure and surface chemistry characterization, Chem. Eng. J., 140 (2008) 32–42.

[17] S. Altenor, B. Carene, E. Emmanuel, J. Lambert, J.J. Ehrhardt, S. Gaspard, Adsorption studies of methylene blue and phenol onto vetiver roots activated carbon prepared by chemical activation, J. Hazard. Mater., 165 (2009) 1029–1039.

[18] H. Yang, R. Yan, H. Chen, D.H. Lee, C. Zheng, Characteristics of hemicellulose, cellulose and lignin pyrolysis, Fuel, 86 (2007) 1781–1788.

[19] E. Raymundo-Pinero, P. Azais, T. Cacciaguerra, D. Cazorla-Amoros, A. Linares-Solano, F. Beguin, KOH and NaOH activation mechanisms of multiwalled carbon nanotubes with different structural organisation, Carbon, 43 (2005) 786–795.

[20] M. Jagtoyen, F. Derbyshire, Activated carbons from yellow poplar and white oak by H_3PO_4 activation, Carbon, 36 (1998) 1085–1097.

[21] Y. Ji, T. Li, L. Zhu, X. Wang, Q. Lin, Preparation of activated carbons by microwave heating KOH activation, Appl. Surf. Sci., 254 (2007) 506–512.

[22] M.A. Lillo-Rodenas, D. Cazorla-Amoros, A. Linares-Solano, Understanding chemical reactions between carbons and NaOH and KOH: An insight into the chemical activation mechanism, Carbon, 41 (2003) 267–275.

[23] M. Uchimiya, L.H. Wartelle, K.T. Klasson, C.A. Fortier, I.M. Lima, Influence of pyrolysis temperature on biochar property and function as a heavy metal sorbent in soil, J. Agric. Food Chem., 59 (2011) 2501–2510.

[24] Y.S. Shen, S.L. Wang, Y.M. Tzou, Y.Y. Yan, W.H. Kuan, Removal of hexavalent Cr by coconut coir and derived chars – The effect of surface functionality, Biores. Technol., 104 (2012) 165–172.

[25] A.C. Lua, T. Yang, Effect of activation temperature on the textural and chemical properties of potassium hydroxide activated carbon prepared from pistachio-nut shell, J. Colloid Interface Sci., 274 (2004) 594–601.

[26] A.M. Puziy, O.I. Poddubnaya, R.P. Socha, J. Gurgul, M. Wisniewski, XPS and NMR studies of phosphoric acid activated carbons, Carbon, 46 (2008) 2113–2123.

[27] M.W. Jung, K.H. Ahn, Y. Lee, K.P. Kim, J.S. Rhee, J.T. Park, K.J. Paeng, Adsorption characteristics of phenol and chlorophenols on granular activated carbons (GAC), Microchem. J., 70 (2001) 123–131.

[28] Y. Lu, C.L. Yan, S.Y. Gao, Preparation and recognition of surface molecularly imprinted core–shell microbeads for protein in aqueous solutions, Appl. Surf. Sci., 255 (2009) 6061–6066.
[29] L. Dupont, E. Guillon, Removal of hexavalent chromium with a lignocellulosic substrate extracted from wheat bran, Environ. Sci. Technol., 37 (2003) 4235–4241.
[30] A.M. Puziy, O.I. Poddubnaya, A.M. Ziatdinov, On the chemical structure of phosphorus compounds in phosphoric acid-activated carbon, Appl. Surf. Sci., 252 (2006) 8036–8038.
[31] Z.H. Jiang, Z. Yang, C.L. So, C.Y. Hse, Rapid prediction of wood crystallinity in *Pinus elliotii* plantation wood by near-infrared spectroscopy, J. Wood. Sci., 53 (2007) 449–453.
[32] J. Hayashi, A. Kazehaya, K. Muroyama, A.P. Watkinson, Preparation of activated carbon from lignin by chemical activation, Carbon, 38 (2000) 1873–1878.
[33] M. Molina-Sabio, F. Rodrigue-Reinoso, Role of chemical activation in the development of carbon porosity, Colloids Surf., A 241 (2004) 15–25.
[34] H. Liu, P. Dai, J. Zhang, C. Zhang, N. Bao, C. Cheng, L. Ren, Preparation and evaluation of activated carbons from lotus stalk with trimethyl phosphate and tributyl phosphate activation for lead removal, Chem. Eng. J., 228 (2013) 425–434.
[35] X. Song, H. Liu, L. Cheng, Y. Qu, Surface modification of coconut-based activated carbon by liquid-phase oxidation and its effects on lead ion adsorption, Desalination, 255 (2010) 78–83.
[36] R.W. Coughlin, F.S. Ezra, Role of surface acidity in the adsorption of organic pollutants on the surface of carbon, Environ. Sci. Technol., 2 (1968) 291–297.
[37] R.S. Juang, F.C. Wu, R.L. Tseng, Adsorption isotherms of phenolic compounds from aqueous solutions onto activated carbon fibers, J. Chem. Eng. Data, 41 (1996) 487–492.